Band structure and infrared optical transitions in ErN

View Online · Export Citation · CrossMark

M. A. McKay,[1] Q. W. Wang,[1] H. A. Al-Atabi,[2,3] Y. Q. Yan,[1] J. Li,[1] J. H. Edgar,[2] J. Y. Lin,[1] and H. X. Jiang[1,a]

AFFILIATIONS

[1]Department of Electrical and Computer Engineering, Texas Tech University, Lubbock, Texas 79409, USA
[2]Tim Taylor Department of Chemical Engineering, Kansas State University, Manhattan, Kansas 66506, USA
[3]Chemical Engineering Department, The University of Technology, PO Box 35010, Baghdad, Iraq

[a]Author to whom correspondence should be addressed: hx.jiang@ttu.edu

ABSTRACT

Erbium nitride (ErN) is a rare-earth metal mononitride with desirable electronic, magnetic, and optical properties. ErN can be incorporated into III-nitride semiconductors to develop new functional materials for optoelectronic and spintronic devices. Here, we report on the optical properties of ErN crystals, grown by sublimation and probed by photoluminescence (PL) spectroscopy. Three transition lines were observed near 1 eV. Theoretically, ErN has a small indirect energy gap of around 0.2 eV with a conduction band minimum at the X-point of the Brillouin zone and a valence band maximum at the Γ-point. The predicted smallest direct energy gap is around 1 eV, with two valence bands at the X-point. Using the PL results together with the reported calculations, a coherent picture for the band structure at the X-point for ErN crystals has been derived. Experimental results revealed that ErN has a minimum direct bandgap of 0.98 eV and a total of two valence bands separated by about 0.37 eV at the X-point.

Published under license by AIP Publishing. https://doi.org/10.1063/5.0006312

Rare-earth metal mononitrides (RENs) are known for their unique magnetic and electrical properties due to their highly localized 4f orbitals.[1] Despite having the same crystalline structure and similar lattice constants, RENs display a wide range of electronic and magnetic properties, making them promising candidates for spintronic devices.[2] RENs can potentially be incorporated into III-nitrides to develop new devices. Their narrow direct bandgap ($\sim$1 eV) has applications in infrared (IR) photonic devices. III-nitride and REN heterojunctions could have desirable application features for multiwavelength photonic devices.[3,4]

One of these RENs is erbium nitride (ErN). ErN forms predominantly in the rock salt cubic phase crystalline structure (like NaCl) with a lattice constant of 4.83 Å.[5] The majority of previous studies on ErN focused on its electrical and magnetic properties. ErN is a semiconductor in its ferromagnetic (FM) phase.[6–8] ErN and rare earth oxides (REOs) have shown to be good candidates as buffer layer materials to enhance the quality of III-nitride material grown on silicon substrates.[4,9] Studies have shown that ErN is a tough material (toughness/fracture ratio = 0.61) and possesses anisotropic thermal conductivity.[10] ErN has also been used as a second stage regenerator of 4 K Gifford–McMahon (GM) cryocoolers due to its large specific heat at cryogenic temperatures (1 J/K cm^3 at 4 K).[11]

Erbium (Er) doped materials have also been intensively studied, both theoretically and experimentally, for their promising applications in areas such as solid-state lasers and optoelectronic devices operating in the retina-safe and fiber optical communication wavelength window of 1.54 μm.[12–34] In particular, the emission lines near 1.54 μm in Er doped GaN (Er:GaN) are due to the 4f intra-subshell transitions of the Er trivalent ions (Er^{3+}) and are very stable with a small thermal quenching effect.[20,21,31,32] Studies of Er doping in Er:GaN have shown that Er ions can be incorporated into thin epitaxial films at concentrations as high as 1%–2% with small thermal quenching.[21] However, achieving Er:GaN bulk crystals with the potential to serve as a robust optical gain medium for high energy lasers with high Er concentrations and high crystalline quality is challenging.[31–34] Due to the larger size of Er atoms compared to that of Ga atoms, the incorporation of Er tends to introduce strains and point defects into Er:GaN. Moreover, due to this atomic size mismatch, a phase transition is expected for Er:GaN when the Er concentration surpasses a critical value since GaN and ErN have different crystalline structures. Therefore, obtaining an improved understanding of the optical transitions and the band structure of pure ErN can be helpful for

understanding the basic growth processes and properties of Er:GaN gain materials as well as for potential applications of ErN.

Despite the growing amount of research, the optical properties of ErN are not yet well known. For example, the energy band structure and exact energy bandgap are still unknown. In this work, we report the properties of the optical transitions in ErN, which were probed by photoluminescence (PL) spectroscopy. By comparing our experimental results with theoretical calculations of the band structure,[1,5,6,8] we present a coherent picture for the band structure and optical transitions of ErN near the X-point of the Brillouin zone.

The ErN crystals were grown by the sublimation-recondensation method in a tungsten furnace heated by a resistive heater via a process that was previously described.[35] Because of the lack of native substrates for REN epitaxial growth and the tendency of rare-earth metals to react with silicon, (100) oriented crystals have been the substrate of choice for most researchers to grow rocksalt crystal structures.[36] The ErN crystals were grown unseeded on two polycrystalline tungsten foil templates with a predominately (100) texture. This foil was cleaned sequentially by acetone, methanol, and isopropyl alcohol. The distance between the ErN source and the growth area was kept constant at approximately 2 cm. The ErN source was synthesized by heating small chunks of Er metal (99% purity) in ultra-high-purity nitrogen at $1500 \,^\circ$C and 400 Torr for 15 h. The ErN crystal growth was carried out at $1810 \,^\circ$C under a nitrogen pressure of 150 Torr. One of the two samples was coated with 10 nm of MgF_2 to prevent its oxidation upon exposure to ambient air. Following the growth, the uncoated samples were immediately sealed in argon jars with a desiccant for future measurements. The MgF_2 coated sample was placed in a regular sample container with no protection from air. The PL system used consists of a 375 nm (3.31 eV) and 16 mW laser diode, a cooled InGaAs camera, and a near-infrared spectrometer from BaySpec Inc.

Figure 1 shows an optical microscope image illustrating the preferential nucleation of ErN crystals at the tungsten foil's grain boundaries, which revealed that ErN tends to have 3D growth and does not form a thin film. ErN adopted a predominately (100) orientation to match the orientation of the tungsten foil.[36] The dark color represents the ErN crystal with average dimensions of $30 \times 10 \times 10 \,\mu m^3$. The density of ErN crystals is approximately 4.6×10^4 individual crystals/cm^2.
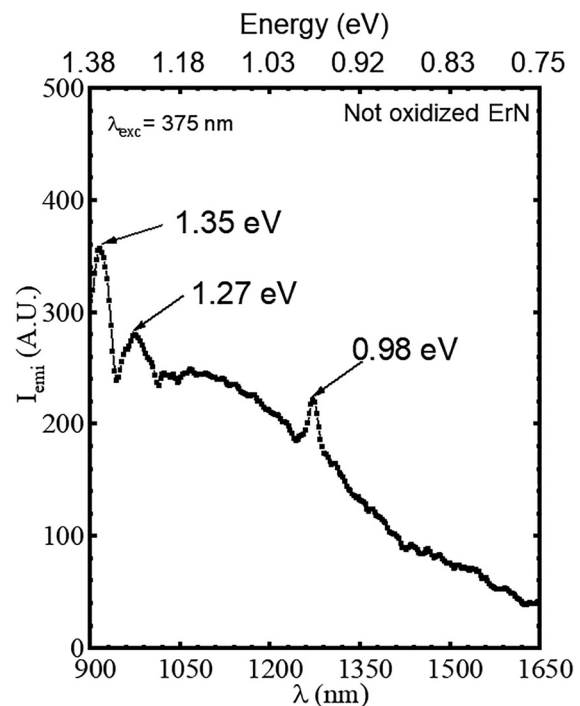
ErN expeditiously oxidizes in Er_2O_3 due to moisture in ambient air,[36,37] and thus, the PL measurements were conducted immediately following the opening of the sample container. Figure 2 shows the measured PL spectrum of ErN at room temperature, covering the
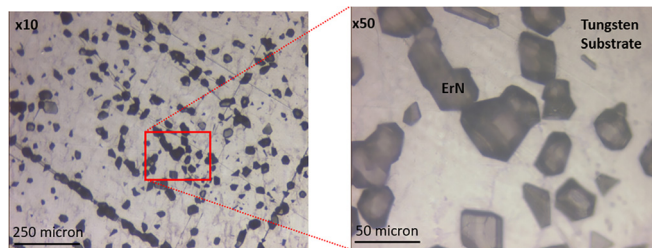
wavelength range of 900 to 1650 nm. Three emission lines with peak positions located at 0.98, 1.27, and 1.35 eV were clearly resolved. There is a large background with its intensity increasing with a decrease in the emission wavelength, which becomes more prevalent with time. The cause of this emission background is unclear at this point.

The emission spectra of the MgF_2 coated sample are shown in Fig. 3(a). The PL spectrum is nearly identical to that of the uncoated sample, with smaller PL intensities due to the top coverlayer of MgF_2. Figure 2 is replotted in Fig. 3(b) for comparison. These two samples have very similar emission features. We performed a series of PL measurements after leaving the uncoated ErN sample in air for 1 and 3 days to study the effects of oxidation. The emission spectra for these measurements are shown in Figs. 3(c) and 3(d). After oxidation, a new peak emerged at around 1534 nm. This 1534 nm peak, of course, is well-known due to the $4f$ intra-subshell transition of Er^{3+} atoms. However, note that the $4f$ intra-subshell transitions of Er^{3+} atoms near $1.54 \,\mu m$ were not observed in ErN. The results show clearly that ErN has been oxidized in air and this 1534 nm line is emitted from Er^{3+} atoms embedded in the newly formed Er_2O_3 on the surface of the ErN crystals. This peak position is consistent with the previously reported Er^{3+} atomic transition peaks in Er_2O_3[37] and is widely recognized and attributed to the intra-$4f$ Er^{3+} transition between $^4I_{13/2} \rightarrow {}^4I_{15/2}$. This addition of two new peaks after oxidation should be noted in any further optical exploration or applications of ErN. Interestingly, the emission peak around 1.27 eV has also been observed previously in Er_2O_3 powders[37] and hence should be excluded from band-to-band transitions in ErN. However, the observation of the 1.27 eV peak seems to

FIG. 1. Microscope image of the ErN crystals grown on the tungsten substrate. The crystals adopted a predominately (100) orientation due to nucleation on the substrate's grain boundaries. The dark color represents the ErN crystal with average dimensions of $30 \times 10 \times 10 \,\mu m^3$. The density of the crystals is approximately 4.6×10^4 individual crystals/cm^2.

FIG. 2. Photoluminescence spectrum of ErN measured at room temperature with the above-bandgap 3.31 eV ($\lambda = 375$ nm) excitation energy. The arrows indicate the energy of the dominant transition peaks.
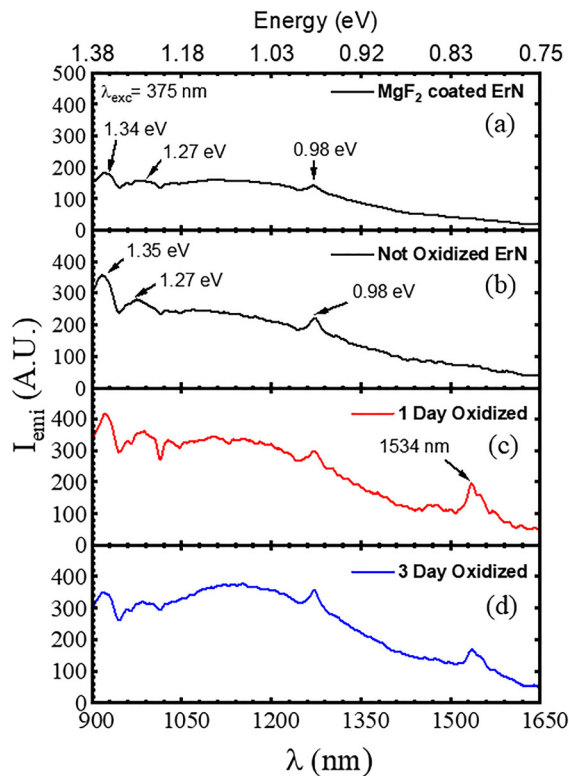
FIG. 3. PL spectra measured at room temperature with the above-bandgap 3.31 eV ($\lambda = 375$ nm) excitation energy of ErN: (a) coated with MgF_2; (b) without coating (replot of Fig. 2); (c) after 1 day of air exposure; and (d) after 3 days of air exposure.

suggest that the material is already affected by oxidization before our first measurement of the uncoated ErN sample as well as before the MgF_2 protective layer was applied to the coated sample.

The band structure of ErN has been previously calculated using various methods.[1,5,6,8] The electronic structures predicted by these different methods were not consistent, mostly at the Γ-point, with a focus on the magnetic properties of ErN. There has been no conclusion on the energy separations between valence bands at the X-point. However, calculations have concluded that the band structure has a small indirect gap of about 0.2 eV, with the conduction band minimum (CBM) at the X-point and the valence band maximum (VBM) at the Γ-point.[1] This indirect bandgap transition is expected to be less efficient and is also outside of our measured spectral range. Calculations also predicted that there are a total of two valence bands at the X-point, which can contribute to band-to-band transitions with an energy separation of around 1 eV between the CBM and the first valence band (A-VB) or a minimum direct energy bandgap. The energy separation between the A-VB and second valence band (B-VB) is around 0.3 eV.[1]

By matching the energy positions of the two main emission peaks at 0.98 and 1.35 eV in our PL results with the calculated electronic structures of ErN,[1] the experimental band structure at the X-point is proposed and is shown in Fig. 4. Based on the calculated band structure,[1] there are two valence bands that contribute to the

band-to-band transitions at the X-point. Our PL results, together with calculations,[1] suggest that the minimum direct energy bandgap is 0.98 eV and the energy separation between the A- and B-valence bands is $1.35 - 0.98 = 0.37$ eV. The measured energy separation between the two valence bands agrees reasonably well with the calculated value of about 0.3 eV.[1] It should be noted that oxygen in ErN can be treated as an impurity (n-type donor). The presence of impurities and defects with a reasonable concentration, such as in this case, is not expected to affect the band structure of the host semiconductor or ErN. Thus, our proposed band structure of ErN will not be affected by the presence of oxygen impurities. This is analogous to the case of Si impurities in GaN. It is well known that the presence of Si donors in GaN will not change the fundamental band structure of GaN. We believe that our experimental results provide useful insights for further improving the calculation results of the band structure of ErN.

In conclusion, we have conducted growth and PL spectroscopy studies of ErN. Two emission lines at 0.98 eV and 1.35 eV observed at room temperature were attributed to the band-to-band transitions. By combining the previously published theoretical band structures and experimental PL spectroscopic results of ErN, we presented a more detailed understanding for the band structure near the X-point and the associated optical transitions in ErN. The PL emission spectra, as ErN oxidizes from air exposure, were also presented. Identification of ErN photoluminescence peaks would help to recognize the presence of the ErN phase and thereby help to improve the growth processes to completely eliminate the ErN phase in Er:GaN bulk crystals. The PL spectroscopic results and the subsequent detailed band structure will
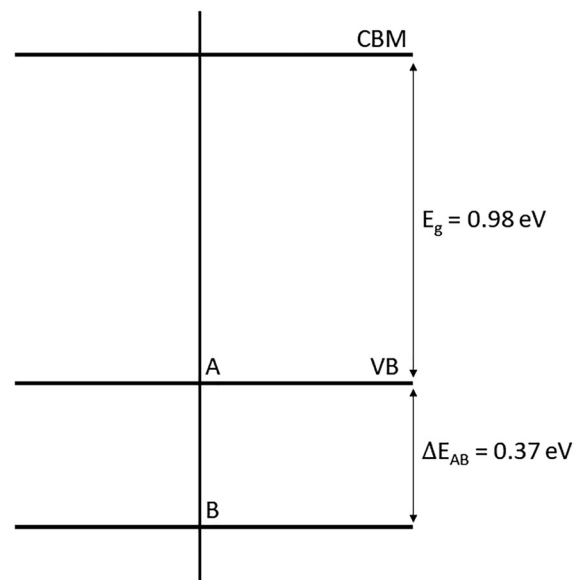
FIG. 4. The proposed band structure of ErN near the X-point of the Brillouin zone that was derived from the measured PL spectra together with the calculated electronic band structures of Ref. 1. The smallest direct energy bandgap of ErN determined from PL spectra is 0.98 eV and is around 1 eV based on the calculated results of Ref. 1.

also help to further understand the basic properties, as well as practical applications in IR and multiwavelength photonic devices of this interesting and less understood material.

The data that support the findings of this study are available within this article.

REFERENCES

[1] P. Larson, W. R. L. Lambrecht, A. Chantis, and M. V. Schilfgaarde, Phys. Rev. B **75**, 045114 (2007).

[2] F. Natali, N. Plank, J. Galipaud, B. Ruck, H. Trodahl, F. Semond, S. Sorieul, and L. Hirsch, J. Cryst. Growth **312**, 3583 (2010).

[3] T. Kent, J. Yang, L. Yang, M. Mills, and R. Myers, Appl. Phys. Lett. **100**, 152111 (2012).

[4] R. Dargis, R. Smith, F. E. Arkun, and A. Clark, Phys. Status Solidi C **11**, 569 (2014).

[5] S. Dergal, A. E. Merad, and B. N. Brahmi, AJMST **2**, 40 (2013).

[6] P. Pandit, V. Srivastava, M. Rajagopalan, and S. P. Sanyal, Physica B **405**, 2245 (2010).

[7] A. G. Petukhov, W. R. L. Lambrecht, and B. Segall, Phys. Rev. B **53**, 4324 (1996).

[8] C. G. Duan, R. F. Sabirianov, W. N. Mei, P. A. Dowben, S. S. Jaswal, and E. Y. Tsmbal, J. Phys. **19**, 315220 (2007).

[9] F. E. Arkun, M. Lebby, R. Dargis, R. Roucka, R. S. Smith, and A. Clark, ECS Trans. **50**, 1065 (2013).

[10] V. Bhalla and D. Singh, Indian J. Pure Appl. Phys. **54**, 40 (2016).

[11] T. Nakagawa, T. Miyauchi, T. Shiraishi, S. Seino, T. A. Yamamoto, Y. Fujimoto, and S. Masuyama, J. Phys. **897**, 012008 (2017).

[12] W. Koechner, *Solid State Laser Engineering*, 3rd ed. (Springer, Berlin, 1992).

[13] W. J. Miniscalco, J. Lightwave Technol. **9**, 234 (1991).

[14] H. Ennen, J. Schneider, G. Pomrenke, and A. Axmann, Appl. Phys. Lett. **43**, 943 (1983).

[15] H. Ennen, G. Pomrenke, A. Axmann, K. Eisele, W. Haydl, and J. Schneider, Appl. Phys. Lett. **46**, 381 (1985).

[16] P. Galtier, J. P. Pochelle, M. N. Charasse, B. deCremoux, J. P. Hirtz, B. Broussin, T. Benyattou, and G. Guillot, Appl. Phys. Lett. **55**, 2105 (1989).

[17] H. Isshiki, H. Kobayashi, S. Yugo, T. Kimura, and T. Ikoma, Jpn. J. Appl. Phys., Part 2 **30**, L225 (1991).

[18] J. Michel, J. L. Benton, R. F. Ferrante, D. C. Jacobson, D. J. Eaglesham, E. A. Fitzgerald, Y. H. Xie, J. M. Poate, and L. C. Kimerling, J. Appl. Phys. **70**, 2672 (1991).

[19] G. Franzo, F. Priolo, S. Coffa, A. Polman, and A. Carnera, Appl. Phys. Lett. **64**, 2235 (1994).

[20] P. N. Favennec, H. L'Haridon, M. Salvi, D. Moutonnet, and Y. Le Guillon, Electron. Lett. **25**, 718 (1989).

[21] C. Ugolini, N. Nepal, J. Y. Lin, H. X. Jiang, and J. M. Zavada, Appl. Phys. Lett. **89**, 151903 (2006).

[22] N. Ter-Gabrielyan, V. Fromzel, X. Mu, H. Meissner, and M. Dubinskii, Opt. Lett. **38**, 2431 (2013).

[23] J. O. White, IEEE J. Quantum Electron. **45**, 1213 (2009).

[24] M. Nemec, J. Sulc, L. Indra, M. Fibrich, and H. Jelınkova, Laser Phys. **25**, 015803 (2015).

[25] T. Sanamyan, J. Opt. Soc. Am. B **33**, D1 (2016).

[26] D. J. Ottaway, L. Harris, and P. J. Veitch, Opt. Express **24**, 15341 (2016).

[27] J. M. Zavada, S. X. Jin, N. Nepal, J. Y. Lin, H. X. Jiang, P. Chow, and B. Hertog, Appl. Phys. Lett. **84**, 1061 (2004).

[28] R. Dahal, C. Ugolini, J. Y. Lin, H. X. Jiang, and J. M. Zavada, Appl. Phys. Lett. **95**, 111109 (2009).

[29] R. Dahal, C. Ugolini, J. Y. Lin, H. X. Jiang, and J. M. Zavada, Appl. Phys. Lett. **97**, 141109 (2010).

[30] D. K. George, M. D. Hawkins, M. McLaren, H. X. Jiang, J. Y. Lin, J. M. Zavada, and N. Q. Vinh, Appl. Phys. Lett. **107**, 171105 (2015).

[31] Z. Y. Sun, J. Li, W. P. Zhao, J. Y. Lin, and H. X. Jiang, Appl. Phys. Lett. **109**, 052101 (2016).

[32] Z. Y. Sun, Q. W. Wang, J. Li, J. Y. Lin, and H. X. Jiang, Proc. SPIE **10528**, 105280E (2018).

[33] Y. Q. Yan, Z. Y. Sun, W. P. Zhao, J. Li, J. Y. Lin, and H. X. Jiang, Appl. Phys. Express **12**, 075505 (2019).

[34] Z. Y. Sun, Y. Q. Yan, T. B. Smith, W. P. Zhao, J. Li, J. Y. Lin, and H. X. Jiang, Appl. Phys. Lett. **114**, 222105 (2019).

[35] Z. Gu, J. H. Edgar, J. Pomeroy, M. Kuball, and D. Coffey, J. Mater. Sci. **15**, 555 (2004).

[36] H. A. Al-Atabi, Z. F. Al Auda, B. Padavala, M. Craig, K. Hohn, and J. H. Edgar, Cryst. Growth Des. **18**(7), 3762 (2018).

[37] E. Nogales, B. Mendez, J. Piqueras, R. Plugaru, A. Coraci, and J. A. García, J. Phys. D **35**, 295 (2002).